applied sciences

MDPI

Article

Modelling Specific Energy Requirement for a Power-Operated Vertical Axis Rotor Type Intra-Row Weeding Tool Using Artificial Neural Network

Satya Prakash Kumar [1,*], V. K. Tewari [2], Abhilash Kumar Chandel [3,*], C. R. Mehta [1], C. M. Pareek [2], C. R. Chethan [4] and Brajesh Nare [5]

[1] Indian Council of Agricultural Research (ICAR)-Central Institute of Agricultural Engineering, Bhopal 462038, India; cr.mehta@icar.gov.in
[2] Indian Institute of Technology, Kharagpur 721302, India; vktfeb@agfe.iitkgp.ac.in (V.K.T.); chaitanyapareek@gmail.com (C.M.P.)
[3] Department of Biological Systems Engineering, Virginia Tech Tidewater, AREC, Suffolk, VA 23437, USA
[4] ICAR-Directorate of Weed Research, Jabalpur 482004, India; chethan.r@icar.gov.in
[5] ICAR-Central Potato Research Station, Jalandhar 144026, India; brajesh.nare@icar.gov.in
* Correspondence: satyaprakash.kr@icar.gov.in (S.P.K.); abhilashchandel@vt.edu (A.K.C.)

Abstract: Specific energy prediction is critically important to enhance field performance of agricultural implements. It enables optimal utilization of tractor power, reduced inefficiencies, and identification of comprehensive inputs for designing energy-efficient implements. In this study, A 3-5-1 artificial neural network (ANN) model was developed to estimate specific energy requirement of a vertical axis rotor type intra-row weeding tool. The depth of operation in soil bed, soil cone index, and forward/implement speed ratio (u/v) were selected as the input variables. Soil bin investigations were conducted using the vertical axis rotor (R_{VA}), interfaced with draft, torque, speed sensors, and data acquisition system to record dynamic forces employed during soil–tool interaction at ranges of different operating parameters. The depth of operation (DO) had the maximum influence on the specific energy requirement of the R_{VA}, followed by the cone index (CI) and the u/v ratio. The developed ANN model was able to predict the specific energy requirements of R_{VA} at high accuracies as indicated by high R^2 (0.91), low RMSE (0.0197) and low MAE (0.0479). Findings highlight the potential of the ANN as an efficient technique for modeling soil–tool interactions under specific experimental conditions. Such estimations will eventually optimize and enhance the performance efficiency of agricultural implements in the field.

Keywords: intra-row weeding; specific energy; artificial neural network; performance efficiency

Citation: Kumar, S.P.; Tewari, V.K.; Chandel, A.K.; Mehta, C.R.; Pareek, C.M.; Chethan, C.R.; Nare, B. Modelling Specific Energy Requirement for a Power-Operated Vertical Axis Rotor Type Intra-Row Weeding Tool Using Artificial Neural Network. *Appl. Sci.* **2023**, *13*, 10084. https://doi.org/10.3390/app131810084

Academic Editors: Paweł Kiełbasa, Anna Miernik and Akinniyi Akinsunmade

Received: 17 July 2023
Revised: 30 August 2023
Accepted: 4 September 2023
Published: 7 September 2023

1. Introduction

Energy is a valuable input in the realm of production agriculture. Availability of adequate and appropriate energy supply, along with its effective and efficient utilization, is essential for a cost-efficient agricultural production. Amongst the agricultural operations, tillage (seed-bed preparation) consumes about 25% of available energy from the prime mover equipment such as tractor. Importantly, fossil fuels account for 92% of this energy supply [1–4]. Numerous studies have examined energy requirements of tractor-implement systems under different operational conditions such as working depth, speed [4–8], soil types, soil moisture, and compaction levels [9]. It has also been claimed that compared to tillage, the intercultural operations such as weeding require more energy [10].

Mechanical weeding is still by far the most deployed method of weeding, although traditionally, weeding tools were pulled by the draft animals and in modern times by self-propelled or tractor machinery. These tools deploy mechanical energy/power derived from chemical energy of the fuels from internal combustion engines to uproot, cut, and bury the weeds. Mechanical weeding tools are intended to control weeds in both inter and

intra-row regions around the crops. The inter-row weeds are those present between the rows while intra-row weeds are the ones between the plants within the rows [11]. Commercially available mechanical weeders can control the inter-row weeds as a standalone operation; however, eradicating intra-row weeds is still a challenge and therefore they are mostly controlled manually. Manual weed control has its own challenges of being tedious, expensive, and inducive of health hazards. The biggest challenge against mechanical weeding of intra-row weeds is avoiding plant damage. Prior studies have reported around 33% of crop yield loss due to mechanical intra-row weeding operations [12–15]. The period of crop-weed competition is 4–5 weeks after plantation and is therefore the instance when the first weeding is recommended, followed by second and third as the need arises. Most importantly, inter-, and intra-row weeding operations are conducted separately. All these frequencies of machinery operations for only weeding operations demand excessive energy and cost requirements, and fossil fuel consumptions thereby endangering production sustainability. In lieu of this situation, an intra-row weeding system that is efficient in operation and results in minimal crop damage is desired. A prototype of a vertical axis rotor weeder (R_{VA}), to eradicate weeds by cutting, uprooting, or mixing in soil was designed and developed.

A sensor-based vertical axis rotor (R_{VA}) type weeder was developed that is simple in design, offers easy attachment and detachment with a tractor. R_{VA} has been suggested to have low tractor draught requirements and losses from rolling resistance and wheel slips. R_{VA} is also a widely used equipment for secondary tillage operation [16–21]. Importantly, vertical axis rotors do not produce tillage hardpans compared to power take-off (PTO)-driven rotary tillers. Furthermore, the soil pulverization capacity of R_{VA} can be adjusted by adjusting the travel and angular speeds of the rotor [22–26].

Energy consumption during a farm operation is one of the most important considerations for researchers, design engineers, and manufacturers when designing/developing agricultural machinery. An optimal management of this energy consumption can optimize fuel consumption and operation costs. This essentially requires design engineers/researchers to have in-depth knowledge of computing specific energy requirements of the soil engaging tool. The specific energy requirements of a soil-engaging tool can be influenced by multiple factors, including the design and operational parameters of the tool and the soil properties. These variables interact in an intricate manner, making the relationships between the specific energy requirement and the input parameters complex and highly non-linear in nature. In a nutshell, modeling specific energy requirements of a soil engaging tool can be a very difficult process using traditional mathematical and statistical methods. Advent of advanced computational and modelling techniques such as machine learning can effectively demonstrate the underlying relationships between input parameters and output as the specific energy. Among such techniques, an artificial neural network (ANN) model was selected to quantify the relationships between specific energy requirement of a soil-engaging tool and operational input parameters. ANN was selected for its superior capability to universally approximate functions, generalizability, and robustness in handling noisy or missing data [27,28]. ANN is well-suited for complex non-linear modelling tasks, particularly when prior knowledge about the input–output relationship is lacking. In the past, researchers have successfully implemented ANN models to quantify soil–tool interactions [29,30].

The energy required to cut weeds and pass through the soil is dependent on design and sharpness of the tool, soil moisture, soil texture, soil specific resistance or compaction level, among others. Therefore, this study was designed to predict the specific energy requirement of a power-operated vertical axis rotor (R_{VA}) type intra-row weeding unit to ultimately aid design and development of tractor-operated weeding tools that are optimal in their power consumption during field operations.

2. Materials and Methods

2.1. Experimental Set-Up

The experimental set-up consisted of a vertical axis rotor (R_{VA})-based weeding prototype unit, an indoor soil bin, soil processing trolley, linear speed transmission system, brushless direct current (BLDC) controller motor, motor controller, tool carriers, load cells, torque transducer, ground wheel with proximity sensor, cone penetrometer, computer, data acquisition system (DAS) and control panel. The overall view of the soil bin facility used for the testing of an intra-row weeding unit is shown in Figure 1.

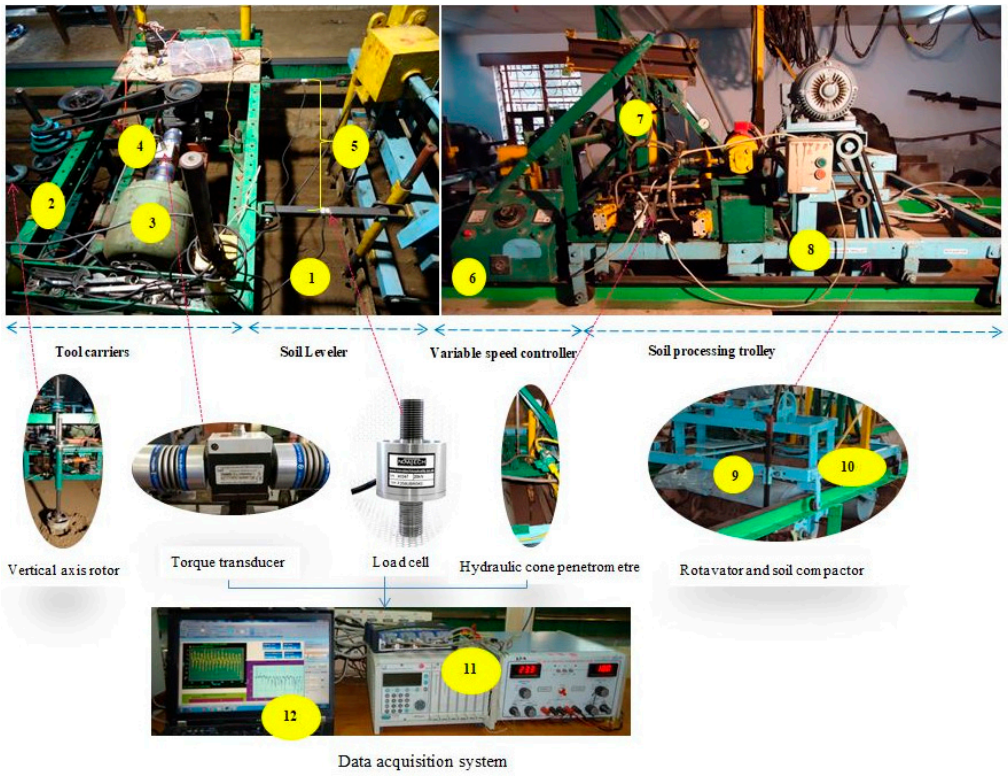

Figure 1. The overall view of the experimental laboratory setup (1. Soil bin; 2. Instrumented tool carrier; 3. BLDC motor; 4. Torque transducer; 5. Load cells; 6. DC motor controller; 7. Hydraulic cone penetrometer; 8. Soil processing trolley; 9. Rotavator; 10. Leveler and Soil compacter; 11. Data acquisition; 12. Laptop computer).

Indoor soil bin was used to simulate variable but known soil conditions like in an actual field. A soil processing trolley was used to prepare the test bed at different soil compaction levels. A linear speed transmission system was used to operate the R_{VA} unit at different forward speeds of operation. The BLDC motor-controller unit was used to control the rotational speed (revolution per minute, rpm) of the R_{VA} unit about the vertical axis. The tool carrier was used to mount the R_{VA} unit along with a suite of sensors. The load cells and torque transducer were used to measure draft and torque of the R_{VA} unit during operations, respectively. The ground wheel with a proximity sensor was used to measure the forward speed of operation, while the hydraulic cone penetrometer was used to measure the cone index (CI, hardness/resistance) of the soil bed. The data acquisition system (DAS) attached to the computer was used to record the real-time data of all sensors and transducers. A control panel was used to control the power supply and actuate all the electrical/electronic equipment. Details of these components are explained in the following sections.

2.1.1. Vertical Axis Rotor Type Intra-Row Weeding Tool

A vertical axis rotor (R_{VA}) was used to destroy the weeds by cutting, uprooting and burying in the soil through the rotary action. The R_{VA} was designed following the standard methods and intra-row zone spacings [31,32]. The diameter of the developed R_{VA} prototype was selected as 120 mm with a thickness of 5 mm. The R_{VA} was moved along the forward direction of travel with rotational motion along the vertical axis as well as side translational motion, perpendicular to the forward travel axis. A trapezoidal-shape tool was selected for weeding operation with a 15° rake angle after extensive design testing [33]. The shape was selected to ensure maximum weed mortality and efficient soil pulverization. Generally, the depth requirement of the weeding operation varies from 20 to 40 mm within three to five weeks after sowing; however, weeding beyond that period may require down to 60 mm of depth. Keeping a 20 mm clearance from the rotor, a length of 80 mm for the cutting tools was selected. High-carbon steel flats of a length of 80 mm, thickness of 3.5 mm and width of 30 mm were selected for fabrication of the cutting tools. Finally, all these cutting tools were mounted on the periphery of a mild steel (MS) ring as shown in Figure 2. The design parameters of tools were calculated by considering required power, speed of operation, R_{VA} rpm, soil parameters, and the width of coverage.

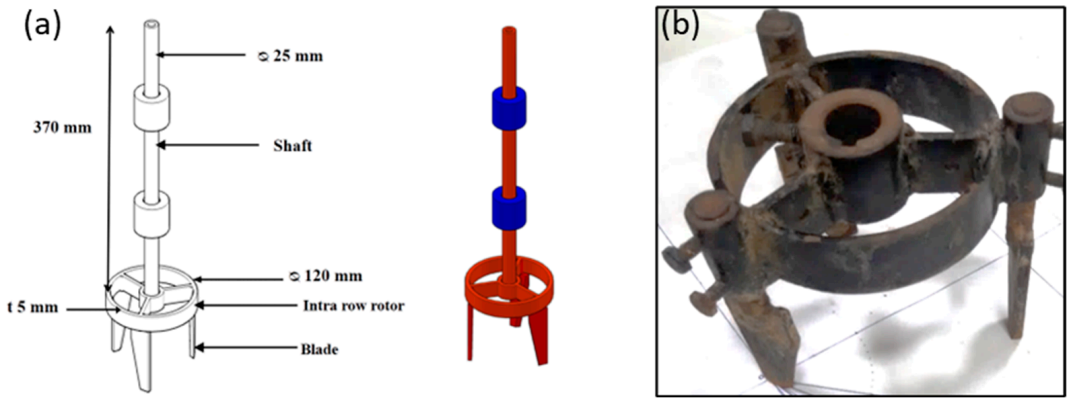

Figure 2. Vertical axis rotor for intra-row weeding: (**a**) CAD view of R_{VA}; (**b**) Developed R_{VA}.

The trajectory of the working element of an R_{VA} unit corresponds to a cycloid (Figure 3). A rigid cutting tool of R_{VA} describes the path of a cycloid when the axis of rotation is perpendicular to the direction of the system's travel [31]. The polar coordinates and the length of soil slices are given in Equations (1) and (2) and discussed below.

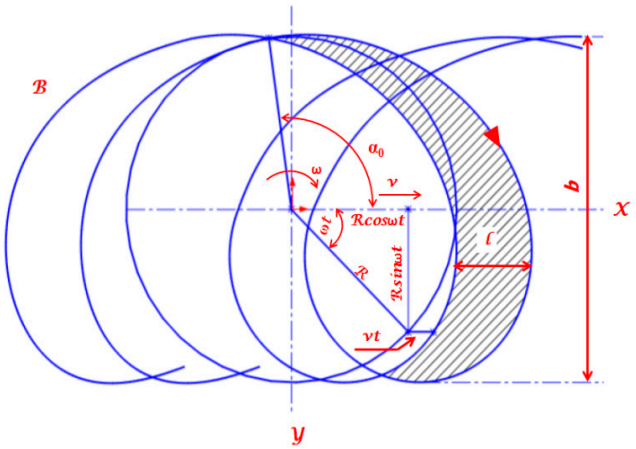

Figure 3. Trajectories of working tools and shapes of soil slices for the vertical axis rotary tool.

For the tool movement, the general equation for converting polar coordinates to cartesian coordinates was used.

For tool 1, $n = 1$, the position is given by:

Xo = 0,

Yo = r.

The parametric equation of a cycloid during motion at the time interval t is given by

$$\begin{aligned} x &= v \times t + r \times cos\omega t, \\ y &= r \times sin\omega t. \end{aligned} \quad (1)$$

Contours of the cut soil slices are limited by two cycloids made by two cutting units operating in succession. The length of soil slices (L) can be calculated as

$$L = \frac{v}{u}\left(\frac{2 \times \pi \times r}{z}\right), \quad (2)$$

where r is the outer radius of the working set (mm); v is the forward speed of travel of the tool (ms^{-1}); ω is the angular speed of the cutting tool set; ωt is the angle of rotation during the measurement time period t; u is the peripheral speed of the cutting tool (ms^{-1}); z refers to the number of tools operating in one plane of cutting. The length of soil slices depends on speed ratio (u/v); the higher the ratio, the shorter the cut soil slice. Therefore, the speed ratio (u/v) was also selected in experimental evaluations of R_{VA}.

2.1.2. Indoor Soil Bin and Processing Unit

A soil bin with dimensions of 23.5 m × 1.37 m × 1.5 m (length × width × depth) was filled with sandy clay loam soil. The soil was taxonomically grouped under Oxyaquic haplustalf (order Alfisol) and it had an angle of internal friction of 22° with particle density of 2.65×10^3 kg m^{-3}. Mild steel angle iron track (size: 90 × 90 × 5 mm^3) was plotted along both sides of the soil bin with the side rails (125 × 65 × 5 mm^3) with a 'C' cross section. The width between the two side rails was 1.37 m. Thus, the movement of soil processing and implement trolley was easily accomplished in the soil bin. The soil processing trolley was used to prepare soil test beds at different compaction levels. The soil processing trolley mainly consists of a hydraulic compacting roller, rotary tiller, and a leveler tool. Soil leveler and compacting roller were used for soil leveling and maintaining compactions. The moisture level of soil was maintained with the help of a water sprinkler, and moisture content was noted for each trial. A 3-phase, 1445 rpm, 3.73 kW-capacity induction motor was used to operate the rotary tiller attachment of the soil processing trolley through pulley and V-belt drive (1:3 and 1:1.5 ratio). An independent drive mechanism was provided for forward and backward movement of the soil processing trolley. The entire operating system was controlled by a control panel placed outside the soil bin.

2.1.3. Weeding Tool Carrier

A rectangular frame/tool carrier of MS channels of 70 × 40 × 5 mm was developed for testing the R_{VA} weeding mechanism. The frame dimensions were 1500 × 610 mm to accommodate all the components pertaining to power transmission and movement of the carrier. The tool carrier was mounted on eight MS rollers (four vertical and four horizontal) to drive the carrier on the bin rails managing load and side thrusts. A sliding rectangular frame of 1220 mm in length and 510 mm in width was fabricated using an MS C-section of 50 × 50 mm for mounting the R_{VA} unit, a DC motor, a torque transducer, load cells and the gear unit. The depth of R_{VA} tools was controlled by moving a pipe slider up and down the tool frame. Rotational power to the R_{VA} shaft in a concurrent mode was provided through the pulley-belt drive system from the DC motor (0.5 kW and 1400 rpm) with rpm control placed on top of the main frame. A compact spur gear box of a 5:1 reduction ratio was used between motor and rotor units. The actual speed of operation was measured using the proximity sensor mounted on a peg type round metallic wheel. The tool carrier was

attached to the soil processing trolley for forward and backward motion like a tractor in the field.

2.2. Instrumentation and Measurement of Inputs and Response Parameters

The soil bed uniformity was tested using the soil cone index (CI) and moisture level measurements before the experiment. The real time travel speed and dynamic force of R_{VA} such as draft, torque and specific energy were also measured with the help of a proximity sensor, a load cell, and a torque transducer, and pertaining responses were recorded in real time using an eight-channel Spider-8 data acquisition system (DAS, HBM QuantumX MX840A, Darmstadt, Germany).

2.2.1. Soil Hardness

A hydraulically operated cone penetrometer (strain gauge, full bridge 350 Ω, 100 kg load carrying capacity) was used to measure the cone index (CI), i.e., soil strength and hardness down to a 150 mm depth from the soil surface as per the procedures detailed in the ASABE Standards S313.3 [34]. Technically, CI is defined as the force per unit base area required to insert a cone-shaped probe into the soil at a steady rate (30 mms^{-1}). The CI probe had a 323 mm^2 of base area and a 30° cone angle. A circular shaft with a 15.6 mm diameter was attached to the CI probe and a ring transducer of 10 kN capacity. The ring transducer converted the actual measured force into an electrical signal and then back to actual force. The ring transducer was equipped with a strain gauge Wheatstone bridge circuit with each gauge of 120 Ω resistance. It was calibrated prior to force measurements. The depth of cone penetration was measured using a rotary potentiometer mounted on a rack-pinion arrangement. The DAS was connected to both the Wheatstone bridge circuit of the ring transducer and the potentiometer. An excitation voltage of 5-volt DC was provided by DAS to the ring transducer [35]. The ring transducer was calibrated by gradually increasing and decreasing the compressive force using dead weights and recording the corresponding output voltage. The CI was recorded before testing the R_{VA} from 10 different locations, 1 m apart along the soil bin to ensure the soil bed uniformity. The soil preparation and compaction measurement procedure was repeated until the selected CI values were achieved for the soil bed.

The soil was prepared down to a depth of 0.5 m and for moisture of 10–12% db. A time-domain-reflectometer moisture probe was used to measure the moisture content of the soil at 10 different locations, 1 m apart in the soil bin. The corresponding soil moisture values were recorded and converted to dry weight basis.

2.2.2. Forward Speed

The actual forward speed of operation was measured by using an inductive type proximity sensor (10–30 V, 15 mm PNP) interfaced with DAS. The peg type ground wheel consisted of a disc on which eight metal strips were attached to generate the pulse from proximity sensor [36]. Counting the total number of metal bids in a given time, the proximity sensor calculated instantaneous forward speed of operation from Equation (3):

$$v = \frac{n \times \pi \times d}{8 \times t}, \quad (3)$$

where v is actual speed of operational (ms^{-1}); d is the diameter of the ground wheel (m); and n is the number of metal bids detected in t seconds.

2.2.3. Draft Force

Cylindrical load cells (Novatech Measurements Limited, East Sussex, UK; F214) were used for measuring the draft force encountered by the rotary tool (R_{VA}) during operation. The rated output of load cells was 1.2 mV/V, the bridge resistance was 350 Ω and the excitation voltage was 10 V. A couple of these load cells were mounted on a single-point dynamometer one end of which was connected to the tool carrier and the other end to

the soil processing trolley. These load cells were also calibrated to identify the sensitivity and linearity in force measurements at different loads. The draft and drawbar power requirements of the developed prototype were calculated using Equations (4) and (5):

$$D = H_1 + H_2, \tag{4}$$

$$DP = D \times v, \tag{5}$$

where D is the draft force (N); H_1 and H_2 are the horizontal components of pull forces (N) measured by load cells 1 and 2, DP is the drawbar power (kW); v is the actual forward speed of operation (ms^{-1}).

2.2.4. Torque

A torque transducer (capacity: 200 Nm for rotational speeds up to 10,000 min^{-1}, rotational speed measurements up to 3000 min^{-1}, HBM Germany, T20WN) was used to determine the torque requirement of the R_{VA} during static as well as dynamic state about the vertical axis at different operating conditions. It also measures rotational speeds or angles of rotation for the turning of static machine parts. The torque transducer unit was horizontally mounted between the prime mover (0.373 kW DC controller motor) and the reduction gearbox that connected to the vertical axis rotor weeding tool. This arrangement is critical to identify continuous dynamic torque requirements. The torque transducer was calibrated prior to deployment and the data were recorded via DAS onto the computer.

2.3. Experimental Design, Data Collection, and Initial Analysis

In this study, speed ratio (u/v), depth of operation (DO), and CI were selected as independent parameters, and the specific energy (SPE) requirement as the dependent parameter. The SPE of the system was calculated from the measured draft and torque (Equation (6)) which is the ratio of equivalent power to the actual field productivity of the implement [24,30,37,38].

$$SPE = \left(\frac{P_r}{\mu_r} + \frac{P_d}{\mu_d}\right) \times \frac{10}{v \times w}, \tag{6}$$

where SPE is specific energy (kWh ha^{-1}); P_r is rotational power (kW); μ_r is transmission efficiency of the rotational motor (assumed to be 0.80); P_d is drawbar power (kW); μ_d is transmission efficiency of the drawbar motor (assumed to be 0.80); v is actual forward speed (km h^{-1}); w is tilled width (m). The weeding tool was tested at three levels of speed ratios (SR: 1.7, 2.2, 3), three depths of operation (DO: 20, 40, 60 mm), three levels of cone Index (CI: 300, 400, 500 $\pm$ 25 kPa) and in three replicates. For the type of soil–tool interaction study presented here, a full factorial design (FFD) experiment was formulated as it is regarded as a highly robust and widely adopted approach for studying main and interaction effects of independent factors on the response as well as using combinations of those input factors for predictive purposes [24,25]. Given three typical conditions of CI, u/v ratio, and DO in the field, a total of 27 combinations were possible. Nonetheless, trials at those 27 input combinations were replicated thrice to obtain 81 datasets that were averaged to 27 datasets for further analysis in the study. The soil bin laboratory experiment is shown in Figure 4. After data collection, initial analysis of variance was conducted to determine the significance of the main and interaction effects of the input parameters on draft, torque and specific energy using the Statistical Package in the Social Sciences (SPSS Inc., Chicago, IL, USA, 1999) at a 5% significance.

(**a**) (**b**) (**c**) (**d**)

Figure 4. (**a**) Test of vertical axis rotor; (**b**–**d**) Soil profiles after operations in soil bin.

2.4. Neural Network Modelling of Specific Energy Requirements

A multilayer feed-forward artificial neural network (ANN) model was used to predict SPE requirement of the rotary weeding unit [28,39]. The model inputs included DO (mm), CI (kPa), and u/v ratio. The trials generated a total of 81 sets of data that were averaged and divided into training (70%) and testing groups (30%). The ANN architecture in this study consisted of three layers of interconnected neurons: the input layer, the hidden layers, and the output layer (Figure 5). The network outputs were obtained by applying activation functions, denoted as *fh* (.) and *fo* (.), to the weighted sum of inputs from the previous layer. The mathematical expression for the *k*th network output was defined using Equation (7).

$$y_k = f_o\left[\sum_{j=1}^{N_h} W_{jk} \cdot f_h\left(\sum_{i=1}^{N_i} W_{ij}x_i + (b_h)_j\right) + (b_o)_k\right], \quad (7)$$

where y_k is the *k*th output variable; x_i is the ith input variable; f_h and f_o are the activation functions in the hidden and the output layers, respectively. *i*, *j*, and *k* denote the input layer, the hidden layer, and the output layer neurons, respectively, and are given as $i = 1, 2 \ldots N_i$; $j = 1, 2 \ldots N_h$ and $k = 1, 2 \ldots N_o$. W_{ij} represents the connection weight between the *i*th input neuron and the *j*th hidden neuron. W_{jk} represents the connection weight between the *j*th hidden neuron and the *k*th output neuron. $(b_h)_j$ denotes the bias for the *j*th neuron in the hidden layer and $(b_o)_k$ is the bias for the *k*th neuron in the output layer. The entire modeling was implemented on a MATLAB R2014b package. An iterative trial and error approach was used to fine-tune the model configuration for optimal neurons. The number of neurons in the input and output layers was determined based on the respective input and output parameters. Consequently, the input layer consisted of three neurons, while the output layer had one neuron. To determine the optimal number of neurons in the hidden layer, a range of one to seven neurons was tested. The criterion for selecting the optimal configuration was based on the minimum mean squared error (*MSE*). By iteratively evaluating different configurations, it was determined that the hidden layer should have five neurons. Hence, the resulting optimal neuron configuration for the ANN model was 3-5-1. The log-sigmoid transfer function (logsig) was used as the activation function in the hidden layer (Equation (8)). For the output layer, the linear transfer function (purelin) was utilized (Equation (9)). The topology of the developed ANN is visually represented in Figure 5. To expedite the training process and ensure fair treatment of all variables during model training, experimental data were normalized using a linear transformation (Equation (10)) [40] within a standardized range of 0.1–0.9 before training.

$$f_h(x) = \frac{1}{(1+e^{-x})}, \; 0 \le f_h(x) \le 1, \quad (8)$$

$$f_o(x) = x, -\infty \leq f_o(x) \leq +\infty, \tag{9}$$

$$x_n = 0.1 + 0.8 \times \left(\frac{x_o - x_{min}}{x_{max} - x_{min}} \right), \tag{10}$$

where x_n and x_o are the normalized and the original values of the input parameters, and x_{max} and x_{min} are the maximum and the minimum values of the input parameters, respectively. During model training, network weights and biases were chosen based on the training dataset by employing the Levenberg–Marquardt backpropagation learning algorithm. To ensure optimal convergence, the maximum number of epochs was set at 1000, while the minimum performance gradient was set at 10^{-7}. Additionally, a damping factor (μ) of 0.001 was applied, and the training process was monitored with a maximum of 6 validation checks before termination. The model underwent rigorous trial and error adjustments to fine-tune the network connection weights, minimizing the mean squared error (MSE) between the predicted and target values of SPE. ANN has been known to perform reliably and robustly even with smaller datasets; for this reason, it was selected for SPE estimations in this study.

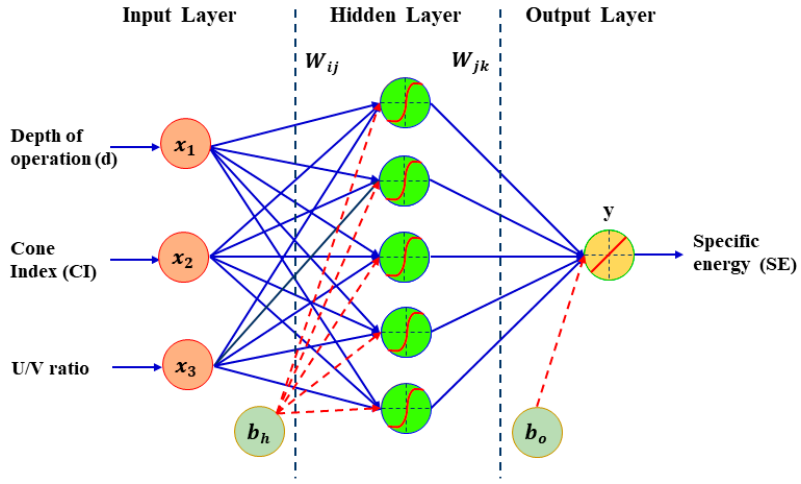

Figure 5. Topology of developed neural network model (x_1, x_2 and x_3 are input variables, and y is estimated output; b_h and b_o are the bias for the hidden layer and the output layer, respectively; W_{ij} and W_{jk} are the connection weights of input hidden layer and hidden output layer, respectively).

To assess the performance of the ANN model, the coefficient of determination (R^2), root mean square error (*RMSE*), and mean absolute error (*MAE*) were used as evaluation metrics [41,42]. These parameters were calculated using Equations (11)–(13):

$$R^2 = \frac{\sum_{i=1}^{N} (O_i - \overline{O}) \times (P_i - \overline{P})}{\sqrt{\sum_{i=1}^{N} (O_i - \overline{O})^2 \times \sum_{i=1}^{N} (P_i - \overline{P})^2}}, \tag{11}$$

$$RMSE = \sqrt{\frac{\sum_{i=1}^{N} (O_i - P_i)^2}{N}}, \tag{12}$$

$$MAE = \frac{1}{N} \sum_{i=1}^{N} |O_i - P_i|, \tag{13}$$

where N is the number of observations, O_i is the observed values, P_i is the predicted values, and the overhead bar (e.g., $\overline{O}$) denotes the mean of the variable.

3. Results

3.1. Effect of Operating Parameters on Specific Energy of R_{VA}

It can be seen from Table 1 that the individual effects of depths, CI, and u/v and their interactions on the specific energy (SPE) were significant with an adjusted R^2 of 0.95, a standard deviation of 0.049 and a coefficient of variation of 12.05%. It can also be identified that the depth of operation (N-way ANOVA, $F_{2,80}$ = 363.5, $p < 0.0001$) had the highest impact on SPE followed by CI ($F_{2,80}$ = 183.19, $p < 0.0001$) and u/v ($F_{2,80}$ = 3.72, $p < 0.05$). It is also clear from the ANOVA table that there was a significant effect of CI on SPE. It can also be seen from this table that CI has higher effect than u/v on SPE. This could be attributed to the volume of soil handled associated with increased operation depth of R_{VA}. The variation of SPE at different operational parameters is shown in Figure 6.

Table 1. Analysis of variance formulated for specific energy of vertical axis rotor (R_{VA}).

Source	Sum of Squares	Degrees of Freedom	Mean Square	F-Value	*p*-Value
Model	2.74	26	0.11	44.18	<0.0001
A: Depth	1.74	2	0.87	363.50	<0.0001
B: Cone index	0.88	2	0.44	183.19	<0.0001
C: u/v	0.013	2	0.0065	3.72	0.03065
A × B	0.055	4	0.0138	5.76	0.0006
A × C	0.025	4	0.00633	2.65	0.0429
B × C	0.020	4	0.00489	2.05	0.1004
A × B × C	0.019	8	0.002385	1.00	0.4484
Error	0.13	54	0.002389		
Total	2.87	80			

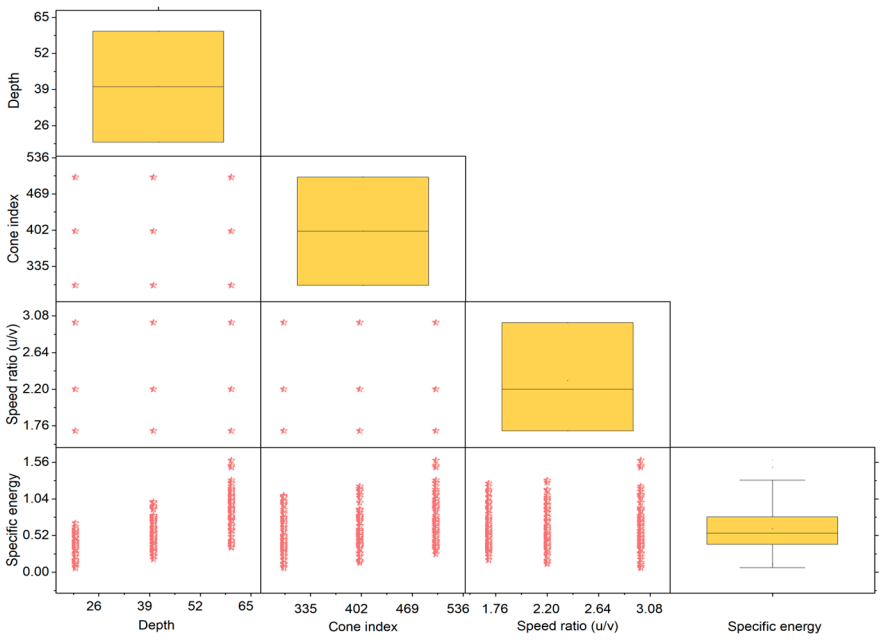

Figure 6. Variation of specific energy at different operational parameters.

3.1.1. Effect of Depth

The results of FFD ANOVA indicate that variation in SPE was dependent on DO ($F_{2,80}$ = 363.5, $p < 0.0001$). As also observed in Figure 7, the SPE of R_{VA} unit increased with the increase in DO. During the trials, the mean SPE required by R_{VA} was in the ranges of 0.061 to 0.87 kWh ha^{-1}. As the DO increased from 20 to 60 mm, SPE increased from 0.19 to 0.45 (SE: ±0.048) kWh ha^{-1}, 0.24 to 0.60 (SE: ±0.053) kWh ha^{-1}, and 0.33 to 0.69 (SE: ±0.059) kWh ha^{-1} at CIs of 300, 400 and 500 kPa, respectively, at the lowest u/v

ratio of 1.7, while at the highest u/v ratio of 3, when the DO increased from 20 to 60 mm, SPE increased from 0.084 to 0.41 (SE: ±0.037) kWh ha^{-1} for CIs of 300 kPa, 0.21 to 0.65 (SE: ±0.063) kWh ha^{-1} for CI of 400 kPa, and 0.34 to 0.73 (SE: ±0.11) kWh ha^{-1} for CI of 500 kPa. As the DO was increased during the trials, SPE increased by 60–70%.

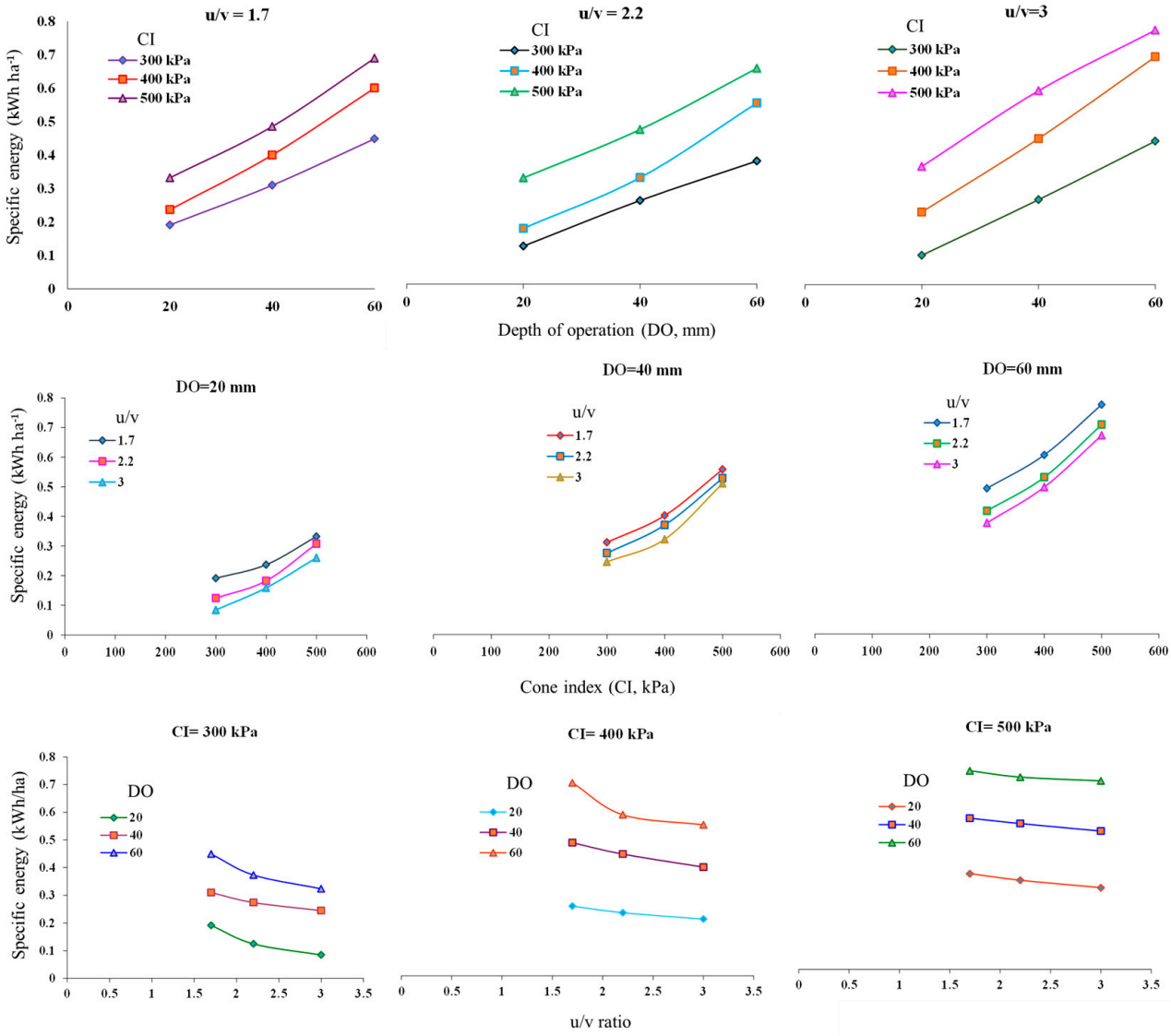

Figure 7. Effect of depth of operation, cone index and u/v ratio on specific energy.

3.1.2. Effect of Cone index

CI had a significant effect on SPE ($F_{2,80}$ = 183.19, $p < 0.0001$). The interaction of DO and CI affected SPE requirements ($F_{4,80}$ = 5.76, p = 0.0006). Figure 7 shows SPE to increase with the increase in CI. As CI was increased from 300-500 kPa, SPE increased from 0.19 to 0.33 (SE: ±0.06) kWh ha^{-1}, 0.12 to 0.30 (SE: ±0.05) kWh ha^{-1}, and 0.08 to 0.26 (SE: ±0.03) kWh ha^{-1} at u/v ratios of 1.7, 2.2, and 3, respectively, at the lowest DO of 20 mm. When CI was increased from 300 to 500 kPa, SPE increased from 0.44 to 0.73 (SE: ±0.11) kWh ha^{-1} for the u/v ratio of 1.7, from 0.41 to 0.70 (SE: ±0.03) kWh ha^{-1} for the u/v ratio of 2.2, and from 0.37 to 0.66 (SE: ±0.07) kWh ha^{-1} for the u/v ratio of 3 for the highest DO of 60 mm.

3.1.3. Effect of u/v Ratio

The speed ratio u/v had a significant effect on SPE ($F_{2,80}$ = 3.72, p = 0.03065) along with the interaction effect of the u/v ratio and DO ($F_{4,80}$ = 2.65, p = 0.0429). SPE decreased in the ranges of 35 to 10% when the u/v ratio increased from 1.7 to 2.2. The variation of SPE

with the u/v ratio at different DOs and CIs is shown in Figure 7. Increasing the u/v ratio from 1.7 to 2.2 resulted in SPE requirements between ranges of 0.19 to 0.08 kWh ha^{-1}, 0.31 to 0.24 kWh ha^{-1}, and 0.44 to 0.32 kWh ha^{-1} at DOs of 20, 40, and 60 mm, respectively, and CI of 300, while when the u/v ratio changed from 1.7 to 3, SPE decreased from 0.35 to 0.30 kWh ha^{-1}, 0.55 to 0.49 kWh ha^{-1} and 0.73 to 0.69 kWh ha^{-1} at selected DO ranges and soil CI of 500 kPa.

3.2. Performance of ANN for Specific Energy Requirement Prediction

A neural network model with a 3-5-1 architecture was formulated to predict specific energy requirements of R_{VA} using three independent variables: DO, CI, and the u/v ratio and Levenberg–Marquardt back-propagation learning. Figure 8a shows the training state of formulated ANN, providing insights into the variation in performance gradient, the Levenberg's damping factor (μ), and the validation check numbers. Notably, the gradient value impressively reduced to 0.0010525 by the 10th epoch, with the μ factor reached 1×10^{-5} at the same epoch. In order to prevent any potential overfitting, the network training was wisely terminated at the 10th epoch, following six validation checks, subsequent to achieving the best validation performance at Epoch 4. As shown in Figure 8b, the best validation performance was obtained at the fourth epoch that yielded the lowest *MSE* of 0.0024612. The regression plots in Figure 9 depict consistency between the predicted and actual SPE requirements from the ANN deployed in this study on training, validation, test, and overall experimental datasets. The correlation coefficients (R) were consistently high, i.e., 0.98666, 0.96029, 0.99294, and 0.97721 for training, testing, validation, and overall datasets, respectively, signifying higher model prediction accuracy.

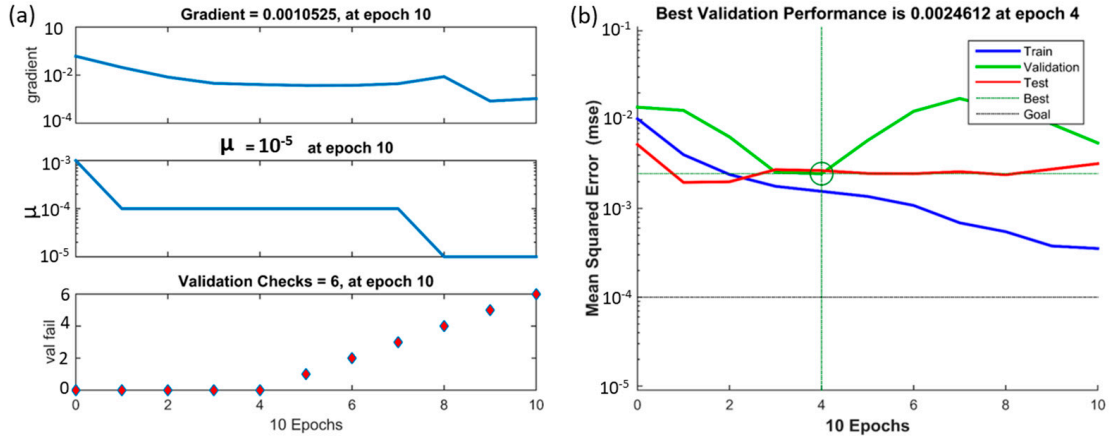

Figure 8. (**a**) Performance curves of formulated ANN model during training and (**b**) curves showing mean square errors during training, testing and validation phases (best performance for MSE of 0.0024612 at 4th training epoch).

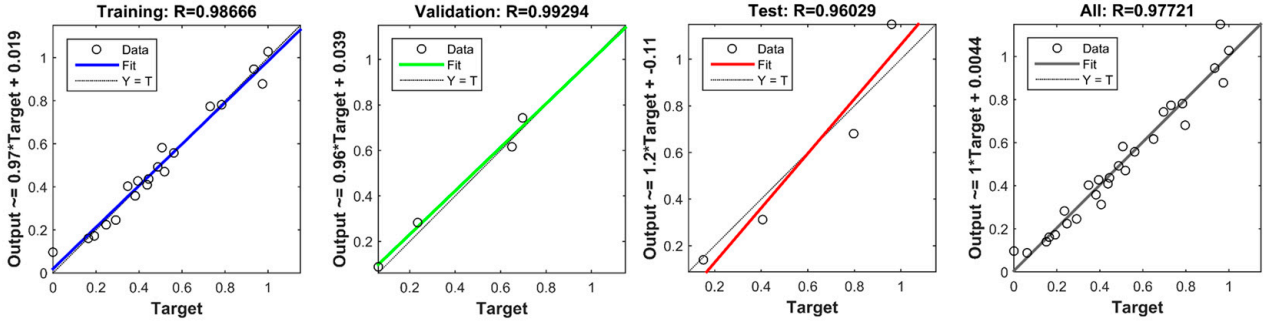

Figure 9. Regression plots of the developed ANN model for different phases.

4. Discussion

4.1. Effect of Input Parameters on Specific Energy

SPE increased in the ranges of 0.19 to 0.69 kWh ha^{-1} at the lowest test range of the u/v ratio and CI, and from 0.34 to 0.73 kWh ha^{-1} for the highest range of the u/v ratio and CI, when DO varied from 20 to 60 mm, respectively. The effect was caused by the increased soil strength brought on by increased DO and the tool interacting with a larger volume of soil, also causing larger draft forces being measured. This was evident in a study by Sahu and Raheman [43] where the draft force increased with the increased forward speed as well as the DO. In this study, SPE also increased with the increase in CI (from 0.44 to 0.73 kWh ha^{-1} for the u/v ratio of 1.7, from 0.41 to 0.70 kWh ha^{-1} for the u/v ratio of 2.2, and from 0.37 to 0.66 (SE: $\pm$0.07) kWh ha^{-1} for the u/v ratio of 3 at the highest DO of 60 mm). This was due to the increase in draft force as the CI increased; since SPE is the function of the draft and torque, it also increased [29,44–50]. A previous study also reported that the draft force requirements of active and passive tillage equipment increased with the increase in CI, u/v ratio, DO, and width of implementation. While the torque requirements only increased when the implement width and CI increased, it decreased with the increase in the u/v ratio and DO [50]. The effect of the u/v ratio and its interaction with DO significantly impacted SPE requirements. When the u/v ratio increased from 1.7 to 2.2, SPE reduced by 35 to 10%. This could be explained by increased accelerating forces due to the rise in u/v which increased draft forces, thereby increasing forces on the soil-engaging tool surface [51,52]. A prior study reported that forward-speed standalone did not significantly impact SPE of tillage implements [30], although it did increase drawbar power requirements as observed in this study.

4.2. Modeling Specific Energy Requirements Using ANN

As shown in Figure 8b, the best validation performance of ANN was obtained at the fourth epoch that yielded the lowest *MSE*. The weights and biases associated with this performance were selected as the final model weights and biases. Although the model training continued until the 10th epoch, as long as the validation error decreased, the training phase was terminated after six consecutive iterations due to an increase in the validation error after the fourth epoch. This was implemented to prevent overfitting. However, the training performance curve did not indicate any overfitting as long as the test and validation curves showed similar trends, which indicates that the training process was robust. The ANN model training exhibited a remarkably high level of regression (R^2 train = 0.9735, Table 2), indicating a strong agreement between the observed and predicted specific energy values. Those values suggest accounting for at least 97% of the variability in specific energy values by the developed ANN model. Similarly, high agreement evident in the testing dataset (R^2 value of 0.9114) suggests that the developed ANN model could account for approximately 91% of the variations at low error and high efficiency in measured specific energy values, even when applied to new independent data (Table 2). This also indicates the generalizability of the developed ANN model. Other studies that have deployed ANN for modeling complex soil–tool interactions [53,54] have also reported ANN to be advantageous for offering fast, precise, and reliable computation of multivariable, nonlinear, and complex relationships relative to mathematical and other conventional numerical methods. This is very well conformed in Figure 10 that illustrates very close alignment between specific energy values measured during experiments and those predicted by the ANN model for each trial in this study. The study by Roul et al. [29] predicted draft forces on a tillage implement using a 5-9-1 ANN model where prediction errors were below 6.5% compared to the standard mathematical equation that estimated draft forces at errors over 30%. Similarly, a 4-6-2 ANN model was used for predicting traction performance and the MSE error was 2.55×10^{-12} [53]. Although the dataset size was relatively smaller, ANN has been well reported to perform reliably and robustly with smaller datasets [55–60]. The next step will be the implementation of the SPE prediction model under various field and vegetation conditions. The developed model and approach

could be instrumental for the manufacturers and design engineers of machinery systems in simulating the designs of soil-interacting tools for operations such as tillage and weeding, among others. Most importantly, such simulation will guide manufacturers to develop matching implements for the tractors to ensure high fuel efficiency, optimal performance, and high crop productivity.

Table 2. Statistical measures of the ANN model performance in training and testing phases.

Statistical Parameters	Training Phase	Testing Phase
R^2	0.9735	0.91139
RMSE	0.00614	0.01974
MAE	0.02247	0.047913

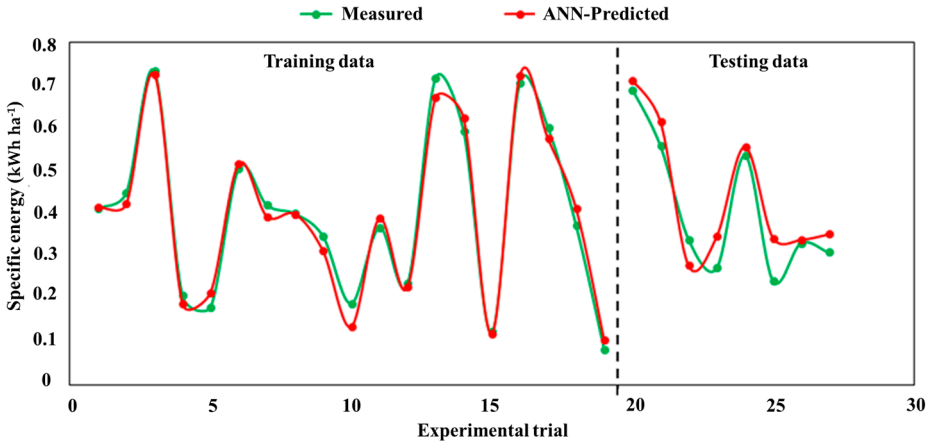

Figure 10. Comparison of measured and ANN-predicted specific energy requirements.

5. Conclusions

An artificial neural network modelling approach was used to predict the specific energy (SPE) requirements of a power operated vertical axis rotor (R_{VA}) type intra-row weeding tool. The depth of operation (DO), cone index (CI), and u/v ratio were considered as the model inputs. The DO had maximum influence on the SPE requirement of the R_{VA} (F-stat: 363.50), followed by the CI (F-stat: 183.19) and the u/v ratio (F-stat: 3.72). A 3-5–1 neural network model was found capable of accurately predicting the specific energy requirement of R_{VA} unit under varying operating conditions as indicated by high R^2 (0.9735), low *RMSE* (0.00614) and low *MAE* (0.0225) for the training phase, as well as for the testing phase (R^2: 0.9114, *RMSE*: 0.0197, *MAE*: 0.0479) on an independent trial dataset. In the soil bin conditions, the chosen factors of DO, CI, and u/v and their levels possibly cover all typical operating conditions which would contribute to suffice reliability of the ANN-based SPE estimations. Importantly, such an estimation approach will guide manufacturers and design engineers to develop matching implements for the tractors and operating conditions to ensure high performance efficiency and crop productivity. Other AI-based modelling techniques such as FIS (Fuzzy Inference System) and ANFIS (Adaptive Neuro-Fuzzy Inference System) will also be employed in future studies to improve the accuracies of SPE predictions. Extensive field trials on different soil types and vegetation conditions will be conducted hereafter.

Author Contributions: Conceptualization, S.P.K. and V.K.T.; methodology, S.P.K., V.K.T. and A.K.C.; software, S.P.K., A.K.C. and B.N.; validation, C.M.P. and C.R.C.; formal analysis, S.P.K.; A.K.C. and C.M.P.; investigation, S.P.K. and A.K.C.; resources, V.K.T.; data curation, S.P.K. and C.M.P.; writing—original draft preparation, S.P.K., C.R.C. and C.M.P.; writing—review and editing, C.R.M. and A.K.C. All authors have read and agreed to the published version of the manuscript.

Funding: This research was supported by the All India Coordinated Research Project on Farm Implements and Machinery, ICAR, Government of India, New Delhi, India.

Institutional Review Board Statement: Not applicable.

Data Availability Statement: Data will be made available on request.

Acknowledgments: The authors are thankful to DDG (Engg), and ADG (F. Engg), ICAR, New Delhi; Project Coordinator, All India Coordinated Research Project on Farm Implements and Machinery for their financial assistance and valuable guidance to conduct this research work.

Conflicts of Interest: The authors declare no conflict of interest.

References

1. Borin, M.; Menini, C.; Sartori, L. Effects of tillage systems on energy and carbon balance in north-eastern Italy. *Soil Tillage Res.* **1997**, *40*, 209–226. [CrossRef]
2. Pimentel, D. *Handbook of Energy Utilization in Agriculture*; CRC Press: Boca Raton, FL, USA, 2019.
3. Choudhury, T.; Kamran, M.; Djajadikerta, H.G.; Sarker, T. Can banks sustain the growth in renewable energy supply? An international evidence. *Eur. J. Dev. Res.* **2021**, *35*, 20–50. [CrossRef]
4. Paris, B.; Vandorou, F.; Balafoutis, A.T.; Vaiopoulos, K.; Kyriakarakos, G.; Manolakos, D.; Papadakis, G. Energy use in open-field agriculture in the EU: A critical review recommending energy efficiency measures and renewable energy sources adoption. *Renew. Sustain. Energy Rev.* **2022**, *158*, 112098. [CrossRef]
5. Godwin, R.J.; O'dogherty, M.J.; Saunders, C.; Balafoutis, A.T. A force prediction model for mouldboard ploughs incorporating the effects of soil characteristic properties, plough geometric factors and ploughing speed. *Biosyst. Eng.* **2007**, *97*, 117–129. [CrossRef]
6. Mattetti, M.; Varani, M.; Molari, G.; Morelli, F. Influence of the speed on soil-pressure over a plough. *Biosyst. Eng.* **2017**, *156*, 136–147. [CrossRef]
7. Balsari, P.; Biglia, A.; Comba, L.; Sacco, D.; Alcatrao, L.E.; Varani, M.; Mattetti, M.; Barge, P.; Tortia, C.; Manzone, M.; et al. Performance analysis of a tractor-power harrow system under different working conditions. *Biosyst. Eng.* **2021**, *202*, 28–41. [CrossRef]
8. Varani, M.; Mattetti, M.; Molari, G.; Biglia, A.; Comba, L. Correlation between power harrow energy demand and tilled soil aggregate dimensions. *Biosyst. Eng.* **2023**, *225*, 54–68. [CrossRef]
9. Natsis, A.; Papadakis, G.; Pitsilis, J. The influence of soil type, soil water and share sharpness of a mouldboard plough on energy consumption, rate of work and tillage quality. *J. Agric. Eng. Res.* **1999**, *72*, 171–176. [CrossRef]
10. Khambalkar, V.; Pohare, J.; Katkhede, S.; Bunde, D.; Dahatonde, S. Energy and economic evaluation of farm operations in crop production. *J. Agric. Sci.* **2010**, *2*, 191–200. [CrossRef]
11. Norremark, M.; Griepentrog, H.W. Physical methods to control weeds within crop rows. In Proceedings of the AgEng—Engineering the Future, Leuven, Belgium, 12–16 September 2004; pp. 1–7.
12. Knezevic, S.Z. The concept of critical period of weed control. In *Integrated Weed Management*; Cooperative Extension; University of Nebraska: Lincoln, NE, USA, 2002; pp. 30–40.
13. Gianessi, L.P.; Reigner, N.P. The value of herbicides in US crop production. *Weed Technol.* **2007**, *21*, 559–566. [CrossRef]
14. Peruzzi, A.; Ginanni, M.; Raffaelli, M.; Fontanelli, M. Physical weed control in organic fennel cultivated in the Fucino Valley (South Italy). In Proceedings of the 7th Workshop of the EWRS Working Group on Physical and Cultural Weed Control, Salem, Germany, 11–14 March 2007; Volume 11, pp. 32–40.
15. Sorensen, C.G.; Norremark, M.; Jørgensen, R.N.; Jensen, K.; Maagaard, J.; Jensen, L.A. Hortibot: Feasibility study of a plant nursing robot performing weeding operations–part IV. In Proceedings of the ASABE Annual International Meeting, Minneapolis, MN, USA, 17–20 June 2007.
16. Chen, Y.; Cavers, C.; Tessier, S.; Monero, F.; Lobb, D. Short-term tillage effects on soil cone index and plant development in a poorly drained, heavy clay soil. *Soil Tillage Res.* **2005**, *82*, 161–171. [CrossRef]
17. Scarlett, A.J. Integrated control of agricultural tractors and implements: A review of potential opportunities relating to cultivation and crop establishment machinery. *Comput. Electron. Agric.* **2001**, *30*, 167–191. [CrossRef]
18. Azadbakht, M.; Azadbakht, B.; Galogah, R.J.; Kiapei, A.; Jafari, H. Soil properties after plowing with horizontal and vertical axis rotavator. *Int. J. Environ. Eng.* **2014**, *8*, 61–65.
19. Makange, N.R.; Tiwari, V.K. Effect of horizontal and vertical axis rotavators on soil physical properties and energy requirement. *Trends Biosci.* **2015**, *8*, 3225–3234.
20. Ganapathi, D.; Duraisamy, V.M.; Shridar, B. Development and optimization of rotary blade for tillage equipment. *Int. J. Agric. Environ. Biotechnol.* **2018**, *11*, 673–677. [CrossRef]
21. Kumar, S.P.; Tewari, V.K.; Chandel, A.K.; Mehta, C.R.; Nare, B.; Chethan, C.R.; Mundhada, K.; Shrivastava, P.; Gupta, C.; Hota, S. A fuzzy logic algorithm derived mechatronic concept prototype for crop damage avoidance during eco-friendly eradication of intra-row weeds. *Artif. Intell. Agric.* **2020**, *4*, 116–126. [CrossRef]
22. Sukcharoenvipharat, W.; Usaborisut, P. Efficiency tests of rotary tiller and power harrow. In Proceedings of the 99th IRES International Conference, Hanoi, Vietnam, 25–26 January 2020.

23. Raparelli, T.; Eula, G.; Ivanov, A.; Pepe, G. Kinematic analysis of rotary harrows. *J. Agric. Eng.* **2020**, *51*, 9–14. [CrossRef]
24. Upadhyay, G.; Raheman, H. Performance of combined offset disc harrow (front active and rear passive set configuration) in soil bin. *J. Terramechanics* **2018**, *78*, 27–37. [CrossRef]
25. Upadhyay, G.; Raheman, H. Comparative assessment of energy requirement and tillage effectiveness of combined (active-passive) and conventional offset disc harrows. *Biosyst. Eng.* **2020**, *198*, 266–279. [CrossRef]
26. Celik, A.; Altikat, S. The effect of power harrow on the wheat residue cover and residue incorporation into the tilled soil layer. *Soil Tillage Res.* **2022**, *215*, 105202. [CrossRef]
27. Haykin, S. *Neural Networks and Learning Machines*, 3rd ed.; Pearson Education India: Noida, India, 2009.
28. Pareek, C.M.; Tewari, V.K.; Machavaram, R.; Nare, B. Optimizing the seed-cell filling performance of an inclined plate seed metering device using integrated ANN-PSO approach. *Artif. Intell. Agric.* **2021**, *5*, 1–12. [CrossRef]
29. Roul, A.K.; Raheman, H.; Pansare, M.S.; Machavaram, R. Predicting the draught requirement of tillage implements in sandy clay loam soil using an artificial neural network. *Biosyst. Eng.* **2009**, *104*, 476–485. [CrossRef]
30. Usaborisut, P.; Prasertkan, K. Specific energy requirements and soil pulverization of a combined tillage implement. *Heliyon* **2019**, *5*, e02757. [CrossRef] [PubMed]
31. Bernacki, H.; Haman, J.; Kanafojski, C. *Agricultural Machines, Theory and Construction*; Scientific Publications Foreign Co-operation Centre of the CISTEI: Warsaw, Poland, 1972; Volume I, pp. 429–439.
32. Kumar, S.P.; Tewari, V.K.; Chethan, C.R.; Mehta, C.R.; Nare, B.; Chandel, A.K. Development of non-powered self-propelling vertical axis inter row rotary weeder. *Indian J. Weed Sci.* **2019**, *51*, 284–289. [CrossRef]
33. Salar, M.R.; Esehaghbeygi, A.; Hemmat, A.; Kargarpour, H. Draft force requirements of a dual bent blade subsurface tillage implement. *Agric. Eng. Int. CIGR J.* **2017**, *19*, 74–80.
34. *ASAE S313.3*; Soil Cone Penetrometer. ASABE Standards: St. Joseph, MI, USA, 2001.
35. Kumar, A.A.; Tewari, V.K.; Nare, B.; Chetan, C.R.; Srivastava, P.; Kumar, S.P. Embedded digital drive wheel torque indicator for agricultural 2WD tractors. *Comput. Electron. Agric.* **2017**, *139*, 91–102. [CrossRef]
36. Tewari, V.K.; Kumar, A.; Nare, B.; Kumar, S.P.; Tyagi, A. Microcontroller based roller contact type herbicide applicator for weed control under row crops. *Comput. Electron. Agric.* **2014**, *104*, 40–45. [CrossRef]
37. Hendrick, J.G. A powered rotary chisel. *Trans. ASAE* **1980**, *23*, 1349–1352. [CrossRef]
38. Shinners, K.J.; Wilkes, J.M.; England, T.D. Performance characteristics of a tillage machine with active-passive components. *J. Agric. Eng. Res.* **1993**, *55*, 277–297. [CrossRef]
39. Ma, L.; Xie, F.; Liu, D.; Wang, X.; Zhang, Z. An Application of Artificial Neural Network for Predicting Threshing Performance in a Flexible Threshing Device. *Agriculture* **2023**, *13*, 788. [CrossRef]
40. Roy, S.M.; Pareek, C.M.; Machavaram, R.; Mukherjee, C.K. Optimizing the aeration performance of a perforated pooled circular stepped cascade aerator using hybrid ANN-PSO technique. *Inf. Process. Agric.* **2022**, *9*, 533–546. [CrossRef]
41. Kuradusenge, M.; Hitimana, E.; Hanyurwimfura, D.; Rukundo, P.; Mtonga, K.; Mukasine, A.; Uwitonze, C.; Ngabonziza, J.; Uwamahoro, A. Crop yield prediction using machine learning models: Case of Irish potato and maize. *Agriculture* **2023**, *13*, 225. [CrossRef]
42. Pareek, C.M.; Tewari, V.K.; Machavaram, R. Multi-objective optimization of seeding performance of a pneumatic precision seed metering device using integrated ANN-MOPSO approach. *Eng. Appl. Artif. Intell.* **2023**, *117*, 105559. [CrossRef]
43. Sahu, R.K.; Raheman, H. An approach for draft prediction of combination tillage implements in sandy clay loam soil. *Soil Tillage Res.* **2006**, *90*, 145–155. [CrossRef]
44. Glancey, J.L.; Upadhyaya, S.K.; Chancellor, W.J.; Rumsey, J.W. Prediction of agricultural implement draft using an instrumented analog tillage tool. *Soil Tillage Res.* **1996**, *37*, 47–65. [CrossRef]
45. Grisso, R.D.; Yasin, M.; Kocher, M.F. Tillage implement forces operating in silty clay loam. *Trans. ASAE* **1996**, *39*, 1977–1982. [CrossRef]
46. Al-Janobi, A.A.; Al-Suhaibani, S.A. Draft of primary tillage implements in sandy loam soil. *Appl. Eng. Agric.* **1998**, *14*, 343–348. [CrossRef]
47. Gee-Clough, D.; McAllister, M.; Pearson, G.; Evernden, D.W. The empirical prediction of tractor-implement field performance. *J. Terramech.* **1978**, *15*, 81–94. [CrossRef]
48. Upadhyaya, S.K. *Prediction of Tillage Implement Draft*; Paper No. 84-1518; ASAE: St. Joseph, MI, USA, 1984.
49. Hadas, A. Prediction of draft requirement-soil compaction relations in tilling moist soils. *Soil Tillage Res.* **1986**, *8*, 51–64. [CrossRef]
50. Anpat, R.M.; Raheman, H. Investigations on power requirement of activepassive combination tillage implement. *Eng. Agric. Environ. Food* **2017**, *10*, 4–13. [CrossRef]
51. Gill, W.R.; Vanden Berg, G.F. *Soil Dynamics in Tillage and Traction*; Agricultural Handbook No. 316; ARS, USDA: Washington, DC, USA, 1968.
52. Kepner, R.A.; Bainer, R.; Barger, E.L. *Principle of Farm Machinery*, 3rd ed.; The AVI Publishing Company, Inc.: Westport, CT, USA, 1978.
53. Taghavifar, H.; Mardani, A. Application of artificial neural networks for the prediction of traction performance parameters. *J. Saudi Soc. Agric. Sci.* **2014**, *13*, 35–43. [CrossRef]
54. Zhang, Z.X.; Kushwaha, R.L. Applications of neural networks to simulate soil-tool interaction and soil behavior. *Can. Agric. Eng.* **1999**, *41*, 119.

55. Anantachar, M.; Kumar, P.G.; Guruswamy, T. Neural network prediction of performance parameters of an inclined plate seed metering device and its reverse mapping for the determination of optimum design and operational parameters. *Comput. Electron. Agric.* **2010**, *72*, 87–98. [CrossRef]
56. Davim, J.P.; Gaitonde, V.N.; Karnik, S.R. Investigations into the effect of cutting conditions on surface roughness in turning of free machining steel by ANN models. *J. Mater. Process. Technol.* **2008**, *205*, 16–23. [CrossRef]
57. Karazi, S.M.; Issa, A.; Brabazon, D. Comparison of ANN and DoE for the prediction of laser-machined micro-channel dimensions. *Opt. Lasers Eng.* **2009**, *47*, 956–964. [CrossRef]
58. Mondal, N.; Mandal, S.; Mandal, M.C. FPA based optimization of drilling burr using regression analysis and ANN model. *Measurement* **2020**, *152*, 107327. [CrossRef]
59. Kosarac, A.; Mladjenovic, C.; Zeljkovic, M.; Tabakovic, S.; Knezev, M. Neural-network-based approaches for optimization of machining parameters using small dataset. *Materials* **2022**, *15*, 700. [CrossRef]
60. Pandiyan, V.; Caesarendra, W.; Tjahjowidodo, T.; Praveen, G. Predictive modelling and analysis of process parameters on material removal characteristics in abrasive belt grinding process. *Appl. Sci.* **2017**, *7*, 363. [CrossRef]